Spherical Spline Application to Radio Occultation Data

Research article

Ch. Blick^{1*}, W. Freeden^{1†}

1 Geomathematics Group, University of Kaiserslautern, P.O. Box 3049, 67653 Kaiserslautern, Germany

Abstract:

In recent years, the importance of the Radio Occultation Method (ROM), an observation procedure of atmospheric quantities such as temperature, density, pressure, and water vapor, increased in value. Based on the global distribution and the high accuracy of the measurements between the Earth's surface up to 35km altitude, ROM offers new perspectives for climate monitoring. In order to compare the measurements, the data have to be visualized. This paper gives the basic definitions and theorems of spline approximation on the sphere. Via its adjustable smoothing parameters, ROM can be suitably adapted to approximate the given data. Further on, it demonstrates, splines as approximation structures realizing a minimal bending energy of their graphs provide a good approximation of the data at hand. Our results demonstrate that spherical spline approximation is an appropriate method to visualize the change over time of a given layer and to illustrate the vertical composition of the Earth's atmosphere. Moreover, ROM enables us to compare the layers of the atmosphere at different points in time as well as the approximation of parameters between the measurements on arbitrary points on the Earth.

Keywords:

Radio occultation • spherical spline • climate monitoring © Versita sp. z o.o.

Received 26-08-2011; accepted 29-09-2011

1. Introduction

Over the past years, discussions about climate change grew in importance. In order to prove or disprove the arguments used in these discussions, a large globally distributed dataset is required. RO (Radio Occultation), a satellite based measuring technique, came into play. RO, first suggested by a group at Stanford University in 1962, was developed in order to provide atmospheric data of distant planets in our solar system. The method provides a globally distributed dataset of vertical profiles of atmospheric parameters such as density, pressure, temperature, and water vapor. Several satellites equipped with these measuring instruments were launched into the Earth's atmosphere, one of them the German CHAllenging Minisatellite Payload (CHAMP) provided

the data used in this paper. CHAMP was launched in July 2000 and collected the first measurements in February 2001. CHAMP operated until September 2010 and collected measurements over the whole operating period.

ROM has several advantages over other measuring techniques to obtain atmospheric data in comparison to radiosondes and aircraft based measurement techniques. These benefits consist of weather independency of the measuring technique, global distribution of the data from the Earth's surface up to 35km altitude and high precision.

In order to compare the climate data provided by ROM, the data have to be visualized via mathematical methods. The procedures applied so far such as binning and linear interpolation ([16], [2] and [14]) provide results but don't produce a smooth approximating function. Interpolation by higher order polynomials tend to oscillate which is not desired in scattered data approximation. The purpose of this paper is to introduce spherical splines which are applied to the data provided by CHAMP. So far, spherical splines



^{*}E-mail: blick@mathematik.uni-kl.de

[†]E-mail: freeden@mathematik.uni-kl.de

with respect to the Laplace- Beltrami operator were hard to calculate since there computation involved the evaluation of the Green function of the iterated Beltrami operator given only as a bilinear series ([3]). We use the fact, that the bilinear function has an explicit representation, which shortens the computation time immensely and makes spherical splines numerically and economically efficient. To demonstrate the effectiveness of the approximation method, the (spline) distribution of atmospheric parameters for a specific layer is visualized. The visualization consists of several illustrations, which show the vertical composition of the Earth's atmosphere. In addition, the spline approximation method is applied to document the difference in climate change over different years at the same layer. ROM using spherical splines is successfully applied to compute vertical profiles of atmospheric parameters at positions between the measurements.

The notational background used for the description of ROM follows the conventional approach to be found in the literature. The spherical spline approximation is based on the mathematical settings introduced by [6].

2. Experimental procedure

2.1. Physical Background of ROM

The Radio Occultation method is a measuring technique in planet research, which probes the atmosphere of a planet in order to retrieve atmospheric parameters. In 1962, the method was first suggested by a group at Stanford University during the preparation of NASA's Mars missions Marianer 3 and 4 [19], [12]. Today, the ROM is an important tool in remote sensing of the atmosphere of distant planets and the Earth itself. Nearly every planet in our solar system, including some of the moons and ring systems, has been probed with the aid of Radio Occultation Missions.

The method was applied on Earth via Low Earth Orbiters (LEOs, 400-1300km altitude), which were equipped with a GPS receiver in order to measure signals send out by GPS satellites at 20,000km altitude. The first GPS Radio Occultation concept has been successfully applied by the GPS/MET (MicroLab-1) experiment in 1995 [17]. Due to the success of the GPS/MET experiment, the German CHAllenging Minisatellite Payload (CHAMP, launched in July 2000) [13], and Argentina's SAC-C (launched in November 2000) were set into space, which carried a new generation of GPS-flight receivers ("Blackjack"). These satellites provide quasi-continuous GPS Occultation measurements. Further on, the US-German GRACE mission (launched in March 2002) and the Taiwan-U.S. multi-satellite Constellation Observing System for Meteorology, Lonosphere and Climate (COSMIC, launched in April 2006) [1] provide additional opportunities for continuous observation of the Earth's atmosphere.

The basic idea to retrieve atmospheric parameters is to measure the bending angle and phase delay due to the Doppler Shift of the GPS signal, while the LEO is setting or rising above the Earth's atmosphere, see Figure 1. From these measurements, temperature, density, pressure and water vapor can be calculated by assuming appropriate boundary conditions.

In order to give a basic understanding of the GPS-Radio Occultation method a simplification consists of the assumption of a spherical symmetric distributed atmosphere in order to apply Snell's law and the assumption, that not more than one ray arrives at every observation point on the LEO trajectory. This method is straight forward and is usually applied in regions with no multi path effects such as in the upper troposphere and stratosphere. For more information about the methods used in multi path regions as well as correction methods the reader is referred, e.g., to [18], [7] and [10].

In geometric optics, the path of an electromagnetic wave is modeled as rays connecting the transmitter and receiver of the wave. Assuming a spherical symmetrically distributed atmosphere described by Snell's law, the measured Doppler frequency along the orbit of the LEO is used to compute the incident ray direction at each point on the orbit. Via geometric considerations, the bending angel α of the ray can be computed. The bending angel will be dependent on the *impact factor p* which is a specific constant for each ray. Thereafter, an inverse Abel-transformation is applied in order to calculate the refractive index of the Earth's atmosphere, finally followed by the calculation of atmospheric pressure, density, temperature and humidity.

The equations and calculations leading to the equation of the *refractive index* can be found in either [18] or [7]. The equation for the refractive index reads,

$$n(r_0) = \exp\left[\frac{1}{\pi} \int_{p=p_0}^{p=\infty} \frac{\alpha(p)}{\sqrt{p^2 - p_0^2}} dp\right],\tag{1}$$

where p denotes the impact factor and α the bending angle.

Since the gas in the Earth's atmosphere has a refractive index close to 1, the *refractivity* N is defined via $N=(n-1)\times 10^6$. Different gases contribute differently to the refractivity of the atmosphere. Assuming a neutral atmosphere, the refractivity can be expressed as a function of pressure, temperature and humidity content. In meteorology, the equation for the refractivity is often given as

$$N = c_1 \frac{P}{T} + c_2 \frac{P_w}{T^2}.$$
 (2)

Here, T is the atmospheric temperature given in Kelvin and P represents the total atmospheric pressure, whereas P_w represents the partial pressure of the water vapor in the atmosphere. The pressure is given in hPa. The constants are usually valid for radio frequencies less than 20GHz and have the values $c_1 = 77.60$ and $c_2 = 3.73 \times 10^5$. The equation is also known as the Smith-Weintraub equation [15]. In the neutral atmosphere, the dry as well as the moist air contribute to the total refractivity. Especially in the lower part of the atmosphere and in tropic regions, the moist

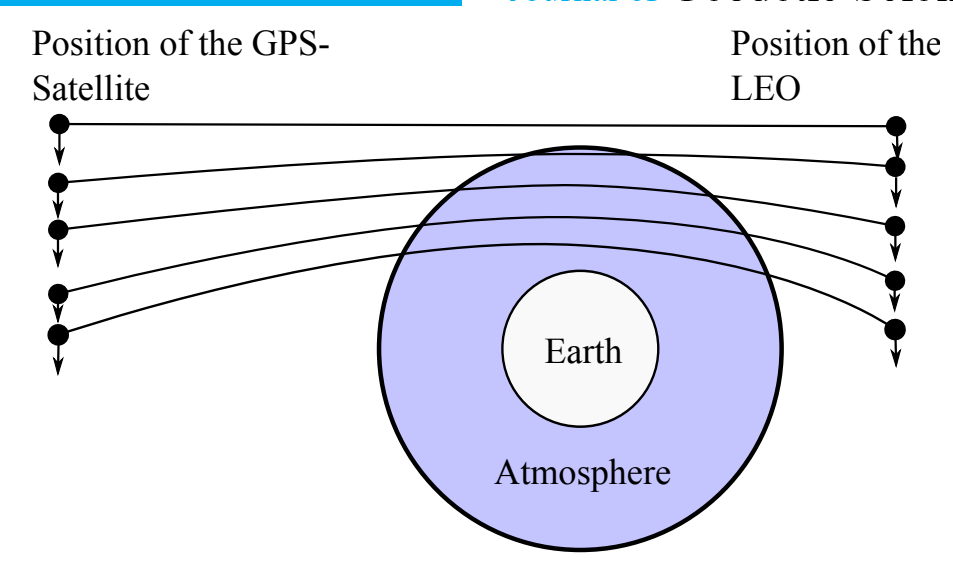


Figure 1. Exemplary position of the two satellites during one occultation

air contributes to a large part of the refractivity and should be considered carefully. For the upper atmosphere and regions, where the moist air has a negligible effect, the atmospheric parameters can be derived easily from Equation (2) with the help of the ideal gas law:

$$P = \frac{\rho RT}{m} = \rho R_m T, \qquad R_m = \frac{R}{m}, \qquad (3)$$

 ρ is the air density, R is the universal gas constant ($R=8.3155 Jmol^{-1}K^{-1}$), m the mean molecular mass of the gas and R_m the specific gas constant.

Assuming that the air is dry, Equation (2) simplifies to

$$N = c_1 \frac{P}{T}. (4)$$

The simplification (4) is necessary in order to calculate atmospheric parameters without further knowledge about current atmospheric conditions and leads to only small errors in the upper troposphere and stratosphere. After combining (4) with (3), an equation for the Earth's density is obtained by

$$\rho_d(z) = \frac{m_d}{Rc_1} N(z), \tag{5}$$

where *z* indicates the height above a reference surface. Further on, inserting Equation (5) in the hydrostatic equation, which is given by

$$\frac{\partial P}{\partial z} = -\rho(z)g(z),\tag{6}$$

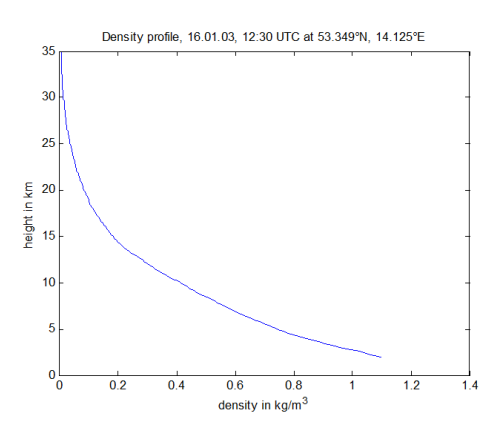


Figure 2. Example of a density profile near Berlin, Germany

where g(z) is the gravity acceleration at height z and finally integrating Equation (6) leads to a representation of the atmospheric pressure:

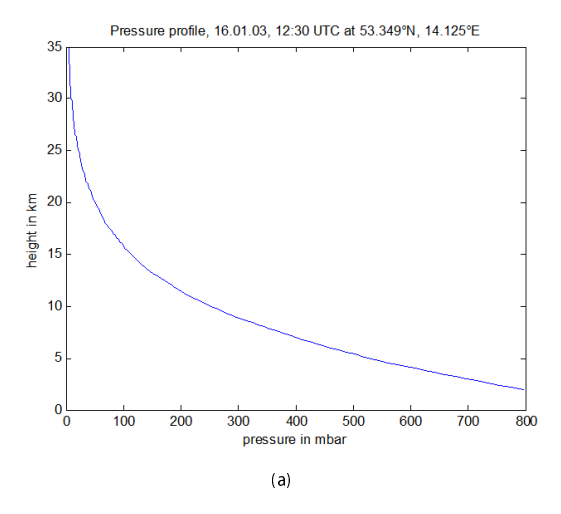
$$P(z) = \int_{z}^{\infty} g(z')\rho_{d}(z')dz' = \frac{m_{d}}{Rc_{1}} \int_{z}^{\infty} g(z')N(z')dz'. \quad (7)$$

Inserting the last result into Equation (4) yields an equation for the atmosphere's temperature:

$$T(z) = \frac{m_d}{RN(z)} \int_z^{\infty} g(z')N(z')dz'. \tag{8}$$

With the help of (5), (7) and (8), atmospheric parameters can be derived from the refractivity profile under the assumption of a dry





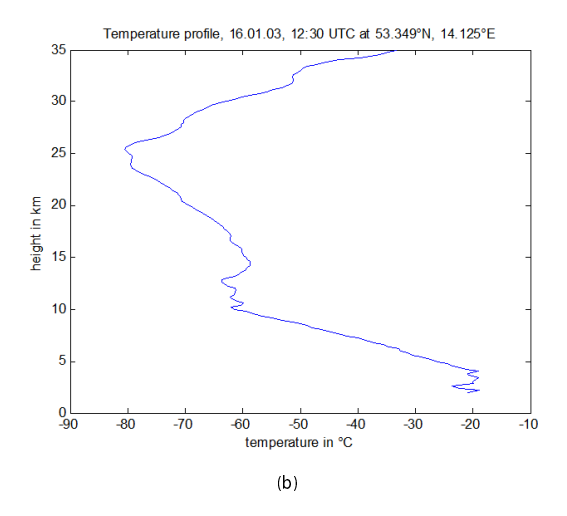


Figure 3. Exemplary pressure (a) and temperature profiles (b) near Berlin, Germany

at mosphere.

Until now, we neglected the water vapor in the Earth's atmosphere. This can be done with small error in the upper troposphere and stratosphere. For the lower troposphere and the warmer tropical regions, the water vapor contributes significantly to the refractivity and can be up to 30% of the total refractivity. Hence, it cannot be neglected. In order to calculate the exact density, pressure and temperature, the water vapor pressure P_w is required. From Equation (2) it can be seen that it is not possible to calculate the atmospheric parameters without independent or a priori information. Such independent information may come from the NCEP (National Center for Environmental Prediction) or ECMWF (European Center for Medium-range Weather Forecast) meteorological analyses or forecast models. Further on, the hydrostatic equation can only be applied to the total pressure.

By use of the prior equations, an iterative process [8] can be applied in order to calculate water vapor profiles. However, this algorithm suffers from a high sensitivity to even small errors in the analyzed temperatures, which result in large uncertainties of the derived water vapor profiles [11].

Inserting Equation (3) into Equation (6) and subsequent integration leads to

$$P(z) = P(z^*) \exp \left(\int_{z}^{z^*} \frac{g(z')}{R_d T_v(z')} dz' \right).$$
 (9)

After reordering Equation (2), $P_w(z)$ can be calculated, if P(z) is known:

$$P_w(z) = T^2(z) \frac{N(z) - c_1 \frac{P(z)}{T(z)}}{c_2}.$$
 (10)

Based on this result, the *specific humidity* q can be calculated, which is defined as:

$$q(z) = \frac{\epsilon P_w(z)}{P(z) - (1 - \epsilon)P_w(z)},\tag{11}$$

where ϵ is usually given the value of 0.622. The iterative procedure is shown in Figure 4.

2.2. Spherical Spline Approximation

In this section, spherical spline approximation is introduced. In the next section the method is used in order to approximate the RO data provided by the GFZ (GeoForschungsZentrum) Potsdam. The mathematics behind the method is based on a new setting developed in [6], namely the explicit representation of the Green function to the iterated Beltrami operator. It enables us to develop spherical spline approximation in close similarity to the one-dimensional cubic spline approach. The analogy is obvious: The spline is a piecewise polynomial which after certain differentiation becomes singular in its nodal points. The singularity is that of the fundamental solution of the Laplace-Beltrami operator. In other words, in one-dimensional theory, the singularity is just a jump so that the spline is an integrated step function. On the sphere the singularity is of logarithmic nature and splines are integrated logarithmically singular Green's functions.

The advantage of the spherical spline approximation compared to currently applied methods for visualization of Radio Occultation data, such as binning and linear interpolation (e.g. [16], [2] and [14]) is the smoothness of the approximating function. In contrast to polynomial interpolation, undesired oscillations can be avoided. Since the dataset provided by the Radio Occultation method is



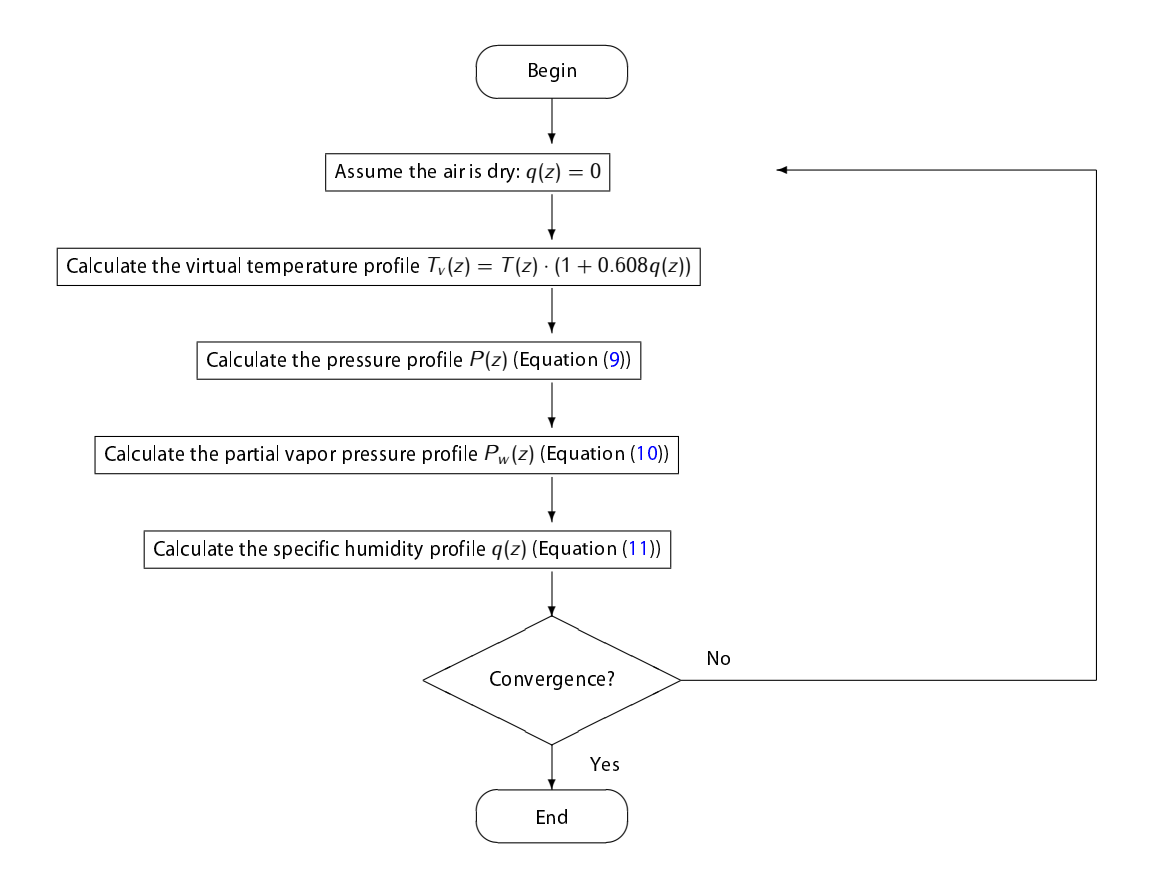


Figure 4. The iterative process for the calculation of the humidity

not dense enough in order to obtain accurate results by the methods mentioned above, this specific method was developed with the intend, that the approximating function prevents undesired oscillations by minimizing the mean curvature.

Up until now, spherical splines were difficult to generate since the entries of the matrix used for its computation (Equation (60)) was approximated by a truncated bilinear series. In this paper, we show, that those entries are given by an explicit formula, which makes the computation of spherical splines numerically and economically efficient.

2.2.1. Notation

In this section, the following notation shall be used: Let \mathbb{R}^3 denote the three dimensional Euclidean space. The variables x, y,... shall be used to denote points in \mathbb{R}^3 with $x=(x_1,x_2,x_3)^T$, $y=(y_1,y_2,y_3)^T$ as their Cartesian coordinates. The *inner*

product and norm are defined as usual via

$$x \cdot y = x_1 y_1 + x_2 y_2 + x_3 y_3, \quad x^2 = x \cdot x, \quad |x| = \sqrt{x^2}.$$
(12)

Using polar coordinates, for all $x\in\mathbb{R}^3$ with $|x|\neq 0$ the following representation can be found:

$$x = r\xi, \qquad r = |x|, \qquad |\xi| = 1.$$
 (13)

The set $\Omega=\{\boldsymbol{\xi}\in\mathbb{R}^3|\,|\boldsymbol{\xi}|=1\}$ denotes the unit sphere with the surface element $d\omega(\boldsymbol{\xi})$.

Let $\bar{\Gamma}$ denote a closed subset of Ω . Then the set $\bar{\Gamma}$ can be decomposed in the following way:

$$\bar{\Gamma} = \Gamma \cup \partial \Gamma, \tag{14}$$

where $\Gamma = \bar{\Gamma} \setminus \partial \Gamma$ is an open set and $\partial \Gamma$ denotes the boundary of $\bar{\Gamma}$. With e_1 , e_2 , e_3 as the canonical orthonormal basis in \mathbb{R}^3 , the points on the unit sphere Ω can be represented by

$$\xi = t\mathbf{e}_3 + \sqrt{1 - t^2}(\mathbf{e}_1 \cos(\phi) + \mathbf{e}_2 \sin(\phi))$$
(15)

with $-1 \le t \le 1$, $-\pi \le \phi < \pi$, $t = \cos(\theta)$, $0 \le \theta \le \pi$. Functions denoted by capital letters F, G, S, \ldots stand for scalar functions, whereas functions denoted by lowercase letters f, g, \ldots shall indicate vector fields. The set of all k-times continuously differentiable scalar functions defined on a set $\mathfrak M$ is denoted by

$$C^{(k)}(\mathfrak{M}),$$
 (16)

whereas the set of all k-times continuously differentiable vector fields defined on a set $\mathfrak M$ is denoted by

$$c^{(k)}(\mathfrak{M}),$$
 (17)

The gradient is defined as

$$\nabla_{\mathbf{x}} = \left(\frac{\partial}{\partial x_1}, \frac{\partial}{\partial x_2}, \frac{\partial}{\partial x_3}\right)^T. \tag{18}$$

Using polar coordinates and the following definitions

$$\boldsymbol{\epsilon}^{r}(\phi, t) = \left(\sqrt{1 - t^{2}}\cos(\phi), \sqrt{1 - t^{2}}\sin(\phi), t\right)^{T},$$

$$\boldsymbol{\epsilon}^{\phi}(\phi, t) = (-\sin(\phi), \cos(\phi), 0)^{T},$$

$$\boldsymbol{\epsilon}^{t}(\phi, t) = \left(-t\cos(\phi), -t\sin(\phi), \sqrt{1 - t^{2}}\right)^{T},$$
(19)

the gradient can be rewritten as

$$\nabla_{x} = \epsilon^{r} \frac{\partial}{\partial r} + \frac{1}{r} \nabla_{\xi}^{*}, \tag{20}$$

where $abla_{\xi}^{*}$ is called *surface gradient* and is defined as:

$$\nabla_{\xi}^* = \epsilon^{\phi} \frac{1}{\sqrt{1 - t^2}} \frac{\partial}{\partial \phi} + \epsilon^t \sqrt{1 - t^2} \frac{\partial}{\partial t}.$$
 (21)

The Laplace-Operator

$$\Delta_{x} = \left(\frac{\partial}{\partial x_{1}}\right)^{2} + \left(\frac{\partial}{\partial x_{2}}\right)^{2} + \left(\frac{\partial}{\partial x_{3}}\right)^{2} \tag{22}$$

can be rewritten by using polar coordinates as

$$\Delta_{x} = \frac{1}{r^{2}} \frac{\partial}{\partial r} r^{2} \frac{\partial}{\partial r} + \frac{1}{r^{2}} \Delta_{\xi}^{*}, \tag{23}$$

where

$$\Delta_{\xi}^* = \frac{\partial}{\partial t} (1 - t^2) \frac{\partial}{\partial t} + \frac{1}{1 - t^2} \left(\frac{\partial}{\partial \phi} \right)^2 \tag{24}$$

denotes the (Laplace-) Beltrami operator on the unit sphere $\Omega.$ The definitions above yield

$$\nabla_{x} \cdot \nabla_{x} = \Delta_{x}$$

$$\nabla_{\xi}^{*} \cdot \nabla_{\xi}^{*} = \Delta_{\xi}^{*}.$$
(25)

VERSITA

2.2.2. Spherical Harmonics

The definitions and theorems in this section are standard material in spherical approximation theory. The proofs for the theorems can be found in either [5] or [6].

Definition 2.1.

Let $n \in \mathbb{N}$ and let $H_n : \mathbb{R}^3 \to \mathbb{R}$ be a homogeneous harmonic polynomial in \mathbb{R}^3 , i.e.

i)
$$\Delta_{\mathbf{x}} H_n(\mathbf{x}) = 0$$
, $\mathbf{x} \in \mathbb{R}^3$

ii)
$$H_n(\mathbf{x}) = H(r\boldsymbol{\xi}) = r^n H_n(\boldsymbol{\xi}), \qquad \boldsymbol{\xi} \in \Omega.$$

Then the function $Y_n: \Omega \to \mathbb{R}$ defined by $Y_n = H_n|_{\Omega}$ is called a spherical harmonic of degree n.

Definition 2.2.

The linear space of all spherical harmonics of degree n is denoted as $\mathbb{H}_n(\Omega)$. By $\mathbb{H}_{0,\dots,m}(\Omega)$ we denote the direct sum of the spaces $\mathbb{H}_0(\Omega) \oplus \dots \oplus \mathbb{H}_m(\Omega)$.

Lemma 2.1.

Every spherical harmonic Y_n of degree n is an everywhere infinitely differentiable eigenfunction of the Beltrami operator Δ^* corresponding to the eigenvalue $\lambda_n = n(n+1)$:

$$(\Delta_{\xi}^* + \lambda_n) Y_n(\xi) = 0, \qquad \xi \in \Omega. \tag{26}$$

The spectrum of Δ_{ε}^* is defined as the set of all eigenvalues:

$$S(\Omega) = \{\lambda_n = n(n+1) \mid n = 0, 1, 2, \ldots\}.$$
 (27)

Remark 2.1.

The collection of all finite linear combinations of elements of the orthogonal direct sum

$$\bigoplus_{n=0}^{\infty} \mathbb{H}_n = \mathbb{H}_0(\Omega) \oplus \mathbb{H}_1(\Omega) \oplus \ldots \oplus \mathbb{H}_m(\Omega) \oplus \ldots$$
 (28)

is dense in the space $C(\Omega)$ of all continuous functions on Ω with respect to the $L^2(\Omega)$ -norm. Moreover, the set is dense in the Hilbert space $L^2(\Omega)$ of all square-integrable functions on Ω .

Lemma 2.2.

There exist 2n+1 linear independent spherical harmonics of degree n. Hence, there exists a set $\{Y_{n,j}\}_{\substack{n=0,1,\dots\\j=1,\dots,2n+1}}^{n=0,1,\dots}$ of spherical harmonics of degree n and order j, which is orthonormal with respect to the inner $L^2(\Omega)$ -product $(\cdot,\cdot)_{L^2(\Omega)}$.

$$(Y_{n,j}, Y_{m,k})_{L^2(\Omega)} = \int_{\Omega} Y_{n,j}(\boldsymbol{\eta}) Y_{m,k}(\boldsymbol{\eta}) d\omega(\boldsymbol{\eta}) = \delta_{nm} \delta_{jk} \quad (29)$$

Moreover, $\{Y_{n,j}\}_{j=1,\dots,2n+1}^{n=0,1,\dots}$ is a closed and complete basis in $L^2(\Omega)$.

Theorem 2.1 (Addition Theorem of Spherical Harmonics).

Let $\{Y_{n,j}\}_{j=1,\dots,2n+1}$ be an orthonormal system in $\mathbb{H}_n(\Omega)$ with respect to $(\cdot,\cdot)_{L^2(\Omega)}$. For any two points ξ , $\eta\in\Omega$ the following equation holds:

$$P_n(\xi \cdot \eta) = \frac{4\pi}{2n+1} \sum_{k=1}^{2n+1} Y_{n,k}(\xi) Y_{n,k}(\eta).$$
 (30)

Here, P_n represents the Legendre polynomial of degree n.

Definition 2.3.

A system η_1,\ldots,η_N of N-points $\eta_k\in\Omega$ with $N\geq M$ is called fundamental system of order m, if the rank of the $M\times N$ - matrix

$$A = \begin{pmatrix} Y_{0,1}(\boldsymbol{\eta}_{1}) & \cdots & Y_{0,1}(\boldsymbol{\eta}_{N}) \\ Y_{1,1}(\boldsymbol{\eta}_{1}) & \cdots & Y_{1,1}(\boldsymbol{\eta}_{N}) \\ \vdots & & \vdots \\ Y_{1,3}(\boldsymbol{\eta}_{1}) & \cdots & Y_{1,3}(\boldsymbol{\eta}_{N}) \\ \vdots & & \vdots \\ Y_{m,1}(\boldsymbol{\eta}_{1}) & \cdots & Y_{m,1}(\boldsymbol{\eta}_{N}) \\ \vdots & & \vdots \\ Y_{m,2m+1}(\boldsymbol{\eta}_{1}) & \cdots & Y_{m,2m+1}(\boldsymbol{\eta}_{N}) \end{pmatrix}$$
(31)

is equal to M.

2.2.3. Green's Function with Respect to the Beltrami Operator

The spherical spline approximation method is based on the theory of Green's function. In this section, Green's function with respect to the Beltrami operator Δ^* shall be introduced. Further on, an exact as well as a bilinear representation shall be discussed. Based on that, Green's function to the iterated Beltrami operator is defined. Its explicit structure and some properties are derived.

Some proofs are not mentioned since the corresponding theorems are well known in the literature, e.g. [5] and [6]. The fundamental part of this section is Lemma 2.6, hence, the proof is given explicitly.

Definition 2.4.

The function $G(\Delta^*; \cdot, \cdot): (\xi, \eta) \mapsto G(\Delta^*; \xi, \eta), -1 \le \xi \cdot \eta < 1$ is called Green's function on Ω with respect to the Beltrami operator Δ^* , if it satisfies the following properties:

i) (Differential equation) for every fixed $\xi \in \Omega$, $\eta \mapsto G(\Delta^*; \xi, \eta)$ is infinitely continuously differentiable on the set $\{\eta \in \Omega | -1 \le \xi \cdot \eta < 1\}$ such that

$$\Delta_{\eta}^* G(\Delta^*; \boldsymbol{\xi}, \boldsymbol{\eta}) = -\frac{1}{4\pi} \qquad -1 \le \boldsymbol{\xi} \cdot \boldsymbol{\eta} < 1. \tag{32}$$

ii) (Characteristic singularity) for every $\xi\in\Omega$, the function

$$\eta \mapsto G(\Delta^*; \boldsymbol{\xi}, \boldsymbol{\eta}) - \frac{1}{4\pi} \ln(1 - \boldsymbol{\xi} \cdot \boldsymbol{\eta}).$$
(33)

Journal of Geodetic Science

is continuously differentiable on Ω .

iii) (Rotational symmetry) for all orthogonal transformations **A** the following equation holds:

$$G(\Delta^*; \mathbf{A}\boldsymbol{\xi}, \mathbf{A}\boldsymbol{\eta}) = G(\Delta^*; \boldsymbol{\xi}, \boldsymbol{\eta}). \tag{34}$$

iv) (Normalization) for every $\boldsymbol{\xi} \in \Omega$ we have

$$\int_{\Omega} G(\Delta^*; \boldsymbol{\xi}, \boldsymbol{\eta}) d\omega(\boldsymbol{\eta}) = 0.$$
 (35)

Lemma 2.3.

The function $G(\Delta^*; \boldsymbol{\xi}, \boldsymbol{\eta})$ is uniquely determined by its defining properties i) - iv)

Theorem 2.2.

Green's function $G(\Delta^*; \boldsymbol{\xi}, \boldsymbol{\eta})$ has the bilinear expansion

$$G(\Delta^*; \boldsymbol{\xi}, \boldsymbol{\eta}) = \frac{1}{4\pi} \sum_{m=1}^{\infty} \frac{2m+1}{\lambda_m} P_m(\boldsymbol{\xi} \cdot \boldsymbol{\eta}), \qquad -1 \le \boldsymbol{\xi} \cdot \boldsymbol{\eta} < 1.$$
(36)

Lemma 2.4.

For ξ , $\eta \in \Omega$ with $-1 \le \xi \cdot \eta < 1$ Green's function with respect to the Beltrami operator Δ^* has the following expression:

$$G(\Delta^*; \boldsymbol{\xi}, \boldsymbol{\eta}) = \frac{1}{4\pi} \ln(2) - \frac{1}{4\pi} \ln(1 - \boldsymbol{\xi} \cdot \boldsymbol{\eta}) - \frac{1}{4\pi}.$$
 (37)

Proof. The function given in the lemma satisfies the definition of Green's function and hence is uniquely determined by Lemma 2.3.

Definition 2.5.

Let $G((\Delta^*)^2; \boldsymbol{\xi}, \boldsymbol{\eta})$ be defined by

$$G((\Delta^*)^2; \boldsymbol{\xi}, \boldsymbol{\eta}) = \int_{\Omega} G(\Delta^*; \boldsymbol{\xi}, \boldsymbol{\zeta}) G(\Delta^*; \boldsymbol{\zeta}, \boldsymbol{\eta}) d\omega(\boldsymbol{\zeta}).$$
 (38)

The function $G((\Delta^*)^2; \boldsymbol{\xi}, \boldsymbol{\eta})$ is called Green's function with respect to the iterated Beltrami operator $(\Delta^*)^2$.

Lemma 2.5.

The bilinear expansion of Green's function to the iterated Beltrami operator reads

$$G((\Delta^*)^2; \boldsymbol{\xi}, \boldsymbol{\eta}) = \frac{1}{4\pi} \sum_{m=1}^{\infty} \frac{2m+1}{\lambda_m^2} P_m(\boldsymbol{\xi} \cdot \boldsymbol{\eta}), \qquad -1 \le \boldsymbol{\xi} \cdot \boldsymbol{\eta} \le 1.$$
(39)

Lemma 2.6.

The Green's function corresponding to the iterated Beltrami operator $(\Delta^*)^2$ is continuous and can be represented in explicit form

$$G((\Delta^*)^2; \boldsymbol{\xi}, \boldsymbol{\eta}) = \begin{cases} \frac{1}{4\pi} &, 1 - \boldsymbol{\xi} \cdot \boldsymbol{\eta} = 0\\ \frac{1}{4\pi} (1 - \ln(1 - \boldsymbol{\xi} \cdot \boldsymbol{\eta}) (\ln(1 + \boldsymbol{\xi} \cdot \boldsymbol{\eta}) - \ln(2)) \\ -\mathfrak{L}_2(\frac{1 - \boldsymbol{\xi} \cdot \boldsymbol{\eta}}{2}) - (\ln(2))^2 + \ln(2) \ln(1 + \boldsymbol{\xi} \cdot \boldsymbol{\eta})) &, 1 \pm \boldsymbol{\xi} \cdot \boldsymbol{\eta} \neq 0, \end{cases}$$

$$\frac{1}{4\pi} - \frac{\pi}{24} &, 1 + \boldsymbol{\xi} \cdot \boldsymbol{\eta} = 0$$

$$(40)$$

where the function \mathfrak{L}_2 is the dilogarithm and it is defined as

$$\mathfrak{L}_{2}(x) = -\int_{0}^{x} \frac{\ln(1-t)}{t} dt = \sum_{k=1}^{\infty} \frac{x^{k}}{k^{2}}.$$
 (41)

Proof. From the bilinear representation of the iterated Green's function (Lemma 2.5) we get

$$G((\Delta^*)^2; \boldsymbol{\xi}, \boldsymbol{\eta}) = \frac{1}{4\pi} \sum_{k=1}^{\infty} \frac{2k+1}{(k(k+1))^2} P_k(\boldsymbol{\xi} \cdot \boldsymbol{\eta}) = \frac{1}{4\pi} \sum_{k=1}^{\infty} \left(\frac{1}{k^2} - \frac{1}{(k+1)^2} \right) P_k(\boldsymbol{\xi} \cdot \boldsymbol{\eta}). \tag{42}$$

Then it follows for all $\xi \in \Omega$:

$$G((\Delta^*)^2; \boldsymbol{\xi}, \boldsymbol{\xi}) = \frac{1}{4\pi} \left(\sum_{k=1}^{\infty} \frac{1}{k^2} - \sum_{k=1}^{\infty} \frac{1}{k^2} + 1 \right) = \frac{1}{4\pi}.$$
 (43)

Further on, we get

$$G((\Delta^*)^2; -\xi, \xi) = \frac{1}{4\pi} \left(\sum_{k=1}^{\infty} \frac{1}{k^2} P_k(-1) - \sum_{k=1}^{\infty} \frac{1}{(k+1)^2} P_k(-1) \right). \tag{44}$$

The well known equation $P_k(-1) = (-1)^k$ leads to:

$$\frac{1}{4\pi} \left(\sum_{k=1}^{\infty} \frac{1}{k^2} P_k(-1) - \sum_{k=1}^{\infty} \frac{1}{(k+1)^2} P_k(-1) \right) = \frac{1}{4\pi} \left(\sum_{k=1}^{\infty} \frac{1}{k^2} (-1)^k - \sum_{k=1}^{\infty} \frac{1}{(k+1)^2} (-1)^k \right)$$
(45)

$$= \frac{1}{4\pi} \left(\underbrace{\sum_{k=1}^{\infty} \frac{1}{k^2} (-1)^k}_{=\frac{\pi^2}{2}} + \underbrace{\sum_{k=1}^{\infty} \frac{1}{k^2} (-1)^k}_{=\frac{\pi^2}{2}} + 1 \right) = \frac{1}{4\pi} - \frac{\pi}{24}.$$
 (46)

 $G(\Delta^*; \boldsymbol{\xi}, \boldsymbol{\eta})$ is a zonal function i.e. the function depends only on the scalar product of $\boldsymbol{\xi}$ and $\boldsymbol{\eta}$. Hence, with $\Delta^*_{\boldsymbol{\xi}}G((\Delta^*)^2; \boldsymbol{\xi}, \boldsymbol{\eta}) = -G(\Delta^*; \boldsymbol{\xi}, \boldsymbol{\eta})$, we get with the help of Lemma 2.4:

$$\frac{d}{dt}(1-t^2)\frac{d}{dt}G((\Delta^*)^2;t) = G(\Delta^*;t) = \frac{1}{4\pi}\ln(1-t) + \frac{1}{4\pi} - \frac{1}{4\pi}\ln(2). \tag{47}$$

Integrating the equation above, we get with the help of the fundamental theorem of integral calculus:

$$\int_{-t}^{t} \frac{d}{d\tau} (1 - \tau^2) \frac{d}{d\tau} G((\Delta^*)^2; \tau) d\tau = (1 - t^2) \frac{d}{dt} G^{(2)}(\Delta^*; t) = -\frac{1}{4\pi} (1 - t) \ln(1 - t) + \frac{\ln(2)}{4\pi} (1 - t). \tag{48}$$

The fundamental theorem of integral calculus and Equation (48) lead further on to:

$$G((\Delta^*)^2; 1) - G((\Delta^*)^2; t) = \int_t^1 \frac{d}{d\tau} G((\Delta^*)^2; \tau) d\tau$$

$$= -\frac{1}{4\pi} \int_t^1 \frac{1}{1+\tau} \ln(1-\tau) d\tau + \frac{\ln(2)}{4\pi} \int_t^1 \frac{1}{1+\tau} d\tau.$$
(49)

By substituting $1 - \tau = u$ in the first integral, we get

$$\frac{1}{4\pi} \int_{t}^{1} \frac{1}{1+\tau} \ln(1-\tau)d\tau + \frac{\ln(2)}{4\pi} \int_{t}^{1} \frac{1}{1+\tau}d\tau = \frac{1}{4\pi} \int_{1-t}^{0} \frac{1}{2-u} \ln(u)du + \frac{\ln(2)}{4\pi} \int_{t}^{1} \frac{1}{1+\tau}d\tau.$$
 (50)

Using a table of integrals [9] we get:

$$\frac{1}{4\pi} \int_{1-t}^{0} \frac{1}{2-u} \ln(u) du + \frac{\ln(2)}{4\pi} \int_{t}^{1} \frac{1}{1+\tau} d\tau
= -\ln(u) \ln\left(\frac{2-u}{2}\right) - \mathcal{L}_{2}\left(\frac{u}{2}\right) + \frac{(\ln(2))^{2}}{4\pi} - \frac{\ln(2)}{4\pi} \ln(1+t),$$
(51)

where the dilogarithm \mathfrak{L}_2 is defined as in Equation (41). With the help of Equation (49) we get

$$G((\Delta^*)^2; 1) - G((\Delta^*)^2; t) = \frac{1}{4\pi} \left(\ln(1-t)(\ln(1+t) - \ln(2)) + \mathfrak{L}_2\left(\frac{1-t}{2}\right) + (\ln(2))^2 - \ln(2)\ln(1+t) \right).$$
(52)

Continuity follows finally from the two equations

$$\lim_{t \to 1} \ln(1-t)(\ln(1+t) - \ln(2)) = 0 \tag{53}$$

and

$$\lim_{t \to -1} (\ln(1-t)(\ln(1+t) - \ln(2)) - \ln(2)\ln(1+t)) = -(\ln(2))^2.$$
(54)

2.2.4. Spherical Spline Functions

Next, spherical splines are defined with the aim to determine the interpolating spline function in a unique way for any given dataset. With the help of the reproducing kernel of the space $H^{(2)}(\Omega)$, which will be defined in this section, it will be shown, that the unique interpolating spline function has a minimum "bending energy". The proofs not stated in this section can be found in e.g. [6], [3] or [4].

Definition 2.6.

In the class of all twice continuously differentiable functions

on Ω , the inner product $(\cdot, \cdot)_H$ is defined by

$$(F,G)_{H} = \int_{\Omega} F(\eta) Y_{0,1}(\eta) d\omega(\eta) \int_{\Omega} G(\eta) Y_{0,1}(\eta) d\omega(\eta) + \int_{\Omega} (\Delta_{\eta}^{*} F(\eta)) (\Delta_{\eta}^{*} G(\eta)) d\omega(\eta)$$
(55)

for all F, $G \in C^{(2)}(\Omega)$. By $H^{(2)}(\Omega)$ we denote the completion of the space $C^{(2)}(\Omega)$ with respect to the norm $\|\cdot\|_H = \sqrt{(\cdot,\cdot)_H}$.

Definition 2.7.

Let the N points η_1, \ldots, η_N be a fundamental system of

VERSITA

388

order 0 on the unit sphere Ω . Then the function

$$S(\boldsymbol{\eta}) = Y_{0,1}(\boldsymbol{\eta}) - \sum_{k=1}^{N} a_k G((\Delta^*)^2; \boldsymbol{\eta}, \boldsymbol{\eta}_k), \qquad \boldsymbol{\eta} \in \Omega, \ c = const. \qquad G((\Delta^*)^2; \boldsymbol{\eta}_i, \boldsymbol{\eta}_k) = \int_{\Omega} G(\Delta^*; \boldsymbol{\eta}_i, \boldsymbol{\zeta}) G(\Delta^*; \boldsymbol{\zeta}, \boldsymbol{\eta}_k) d\omega(\boldsymbol{\zeta}), \quad (63)$$

is called natural spherical spline function in $H^{(2)}(\Omega)$ of order 0 corresponding to the nodes η_1, \ldots, η_N if the vector $a = (a_1, \dots, a_N)^T$ satisfies the linear equation system Aa = 0, where A is given in Definition 2.3. The class of all natural spherical spline functions in $H^{(2)}(\Omega)$ of order 0 corresponding to the nodes η_1, \ldots, η_N is denoted by $\mathcal{S}(\boldsymbol{\eta}_1,\ldots,\boldsymbol{\eta}_N).$

Theorem 2.3.

Let η_1, \ldots, η_N be a fundamental system of order 0 and $y = (y_1, \ldots, y_N)$ be an arbitrary \mathbb{R} -vector. Then there exists a unique spline $S \in \mathcal{S}(\eta_1, \dots, \eta_N)$, such that the equation

$$S(\mathbf{\eta}_k) = \mathbf{y}_k \tag{57}$$

is satisfied for k = 1, ..., N,

The proof of Theorem 2.3 can also be found in the literature given at the beginning of this section but since it reveals the linear equation system which is essential in order to compute the spline function in combination with its explicit solution, the proof is given here.

Proof. We get from the definition of the spline function, that we need to determine N+1 coefficients. For these coefficients we obtain N equations of the following kind:

$$cY_{0,1}(\boldsymbol{\eta}_k) - \sum_{i=1}^{N} a_i G((\Delta^*)^2; \boldsymbol{\eta}_k, \boldsymbol{\eta}_i) = y_k \qquad (k = 1, ..., N).$$
(58)

Equation (58) can be rewritten in matrix formulation via:

$$= \mathbf{A}^T c - \mathbf{G} a = y, \tag{59}$$

where c is a constant, A is defined in Definition 2.3 and G is defined as

$$\mathbf{G} = \begin{pmatrix} G((\Delta^*)^2; \boldsymbol{\eta}_1, \boldsymbol{\eta}_1) & \cdots & G((\Delta^*)^2; \boldsymbol{\eta}_1, \boldsymbol{\eta}_N) \\ \vdots & & \vdots \\ G((\Delta^*)^2; \boldsymbol{\eta}_N, \boldsymbol{\eta}_1) & \cdots & G((\Delta^*)^2; \boldsymbol{\eta}_N, \boldsymbol{\eta}_N) \end{pmatrix}.$$
(60)

The linear equation system

$$Aa = 0 \tag{61}$$

provides one further equation which leads to the $(N+1) \times$ (N+1) equation system

$$\begin{pmatrix} -\mathbf{G} & \mathbf{A}^{\mathsf{T}} \\ \mathbf{A} & 0 \end{pmatrix} \begin{pmatrix} a \\ c \end{pmatrix} = \begin{pmatrix} y \\ 0 \end{pmatrix}. \tag{62}$$

Since

$$G((\Delta^*)^2; \boldsymbol{\eta}_i, \boldsymbol{\eta}_k) = \int_{\Omega} G(\Delta^*; \boldsymbol{\eta}_i, \boldsymbol{\zeta}) G(\Delta^*; \boldsymbol{\zeta}, \boldsymbol{\eta}_k) d\omega(\boldsymbol{\zeta}), \quad (63)$$

the $N \times N$ matrix G is of Gram type. Furthermore, the functions $G((\Delta^*)^2; \eta_1, \eta), \ldots, G((\Delta^*)^2; \eta_N, \eta)$ are linearly independent. Hence det(G) > 0 and we get

$$a = \mathbf{G}^{-1} \mathbf{A}^{T} c - \mathbf{G}^{-1} y$$
 with $c = (\mathbf{A} \mathbf{G}^{-1} \mathbf{A}^{T})^{-1} \mathbf{A} \mathbf{G}^{-1} y$, (64)

which is the unique solution of the linear system.

Theorem 2.4.

The function

$$K(\boldsymbol{\xi}, \boldsymbol{\eta}) = P_0(\boldsymbol{\xi} \cdot \boldsymbol{\eta}) - G((\Delta^*)^2; \boldsymbol{\xi}, \boldsymbol{\eta}) \qquad \boldsymbol{\xi}, \boldsymbol{\eta} \in \Omega \quad (65)$$

is the unique reproducing kernel of the Sobolev space $(H^{(2)}(\Omega), (\cdot, \cdot)_H), i.e.:$

- i) For each fixed $\xi \in \Omega$, $K(\xi, \eta)$ considered as a function of η is an element of $H^{(2)}(\Omega)$.
- ii) For every function $F \in H^{(2)}(\Omega)$ and for every point $\boldsymbol{\xi} \in \Omega$ the reproducing property holds:

$$F(\boldsymbol{\xi}) = (F(\boldsymbol{\eta}), K(\boldsymbol{\xi}, \boldsymbol{\eta}))_{H}. \tag{66}$$

Lemma 2.7.

Let A be given as in Definition 2.3. If the equation Aa = 0 = cis fulfilled, then, for all $S \in \mathcal{S}(\eta_1, \dots, \eta_N)$, i.e. $S(\eta) =$ $cY_{0,1}(\eta) - \sum_{k=1}^N a_k G((\Delta^*)^2; \eta, \eta_k)$, and all $F \in H^{(2)}(\Omega)$, the following equation holds:

$$\int_{\Omega} \Delta_{\eta}^* S(\eta) \Delta_{\eta}^* F(\eta) d\omega(\eta) = \sum_{k=1}^{N} a_k F(\eta_k).$$
 (67)

Theorem 2.5.

Let $(\eta_1, y_1), \ldots, (\eta_N, y_N)$ be N data points, where η_1, \ldots, η_N is a fundamental system of order 0 on Ω . Let $S_N \in$ $S(\eta_1, \ldots, \eta_N)$ be the unique natural spline which interpolates the data points y_1, \ldots, y_N . Then, for all twice continuously differentiable functions F on Ω , which interpolate the data points y_1, \ldots, y_N , the following equation holds true:

$$\int_{\Omega} (\Delta_{\eta}^* S_N(\eta))^2 d\omega(\eta) \le \int_{\Omega} (\Delta_{\eta}^* F(\eta))^2 d\omega(\eta)$$
 (68)

with equality if and only if $F = S_N$,

Proof. From Lemma 2.7 we obtain for every natural spline $S \in \mathcal{S}(\eta_1, \dots, \eta_N)$ the following equation:

$$\int_{\Omega} (\Delta_{\eta}^* S(\eta)) (\Delta_{\eta}^* S(\eta)) d\omega(\eta) = \sum_{k=1}^{N} a_k S(\eta_k).$$
(69)

Combining the equation above with Lemma 2.7 leads to:

$$\int_{\Omega} (\Delta_{\eta}^* S(\eta) - \Delta_{\eta}^* F(\eta))^2 d\omega(\eta) = \sum_{k=1}^N a_k S(\eta_k) - 2 \sum_{k=1}^N a_k F(\eta_k) + \int_{\Omega} (\Delta_{\eta}^* F(\eta))^2 d\omega(\eta). \tag{70}$$

Now let $S_N \in \mathcal{S}$ be the unique interpolating spline. Then, with $F(\eta_k) = y_k = S_N(\eta_k)$ for all k = 1, ..., N, it follows:

$$\int_{\Omega} (\Delta_{\eta}^* S_N(\boldsymbol{\eta}) - \Delta_{\eta}^* F(\boldsymbol{\eta}))^2 d\omega(\boldsymbol{\eta}) = -\sum_{k=1}^N a_k^S F(\boldsymbol{\eta}_k) + \int_{\Omega} (\Delta_{\eta}^* F(\boldsymbol{\eta}))^2 d\omega(\boldsymbol{\eta}), \tag{71}$$

where a_k^S are the coefficients of S_N . From Lemma 2.7 and rearranging the equation above follows:

$$\int_{\Omega} (\Delta_{\eta}^* S_N(\eta))^2 d\omega(\eta) = \int_{\Omega} (\Delta_{\eta}^* F(\eta))^2 d\omega(\eta) - \underbrace{\int_{\Omega} (\Delta_{\eta}^* S_N(\eta) - \Delta_{\eta}^* F(\eta))^2 d\omega(\eta)}_{>0}, \tag{72}$$

which proves the theorem.

Remark 2.2.

Theorem 2.5 suggests that the interpolating spline considered as an infinitesimal thin membrane which is spanned by the data points has minimum bending energy. This interpretation is reflected by the one-dimensional cubic spline interpolation, where the interpolating spline shows minimal "curvature energy" (understood in linearized sense). Furthermore, we do not make an attempt to use splines of orders > 0 (as proposed by [4]). As in the one-dimensional case, higher order splines tend to show more oscillations for a scattered data set, thus, we restrict ourselves to the spherical counterpart of cubic splines.

2.2.5. Smoothing Splines

The interpolating spline function introduced in Section 2.2.4 will be slightly modified in order to allow the smoothing of the data. It turns out that the smoothing spline is still uniquely defined and minimizes a functional that measures the fitness of any approximating function, however, under additional statistically oriented prerequisites.

Definition 2.8.

The problem of fitting a smooth function to a given dataset $(\eta_1, y_1), \dots, (\eta_N, y_N)$ is given by determining a function F,

such that the functional

$$\sigma_{\beta,\delta}(F) = \sum_{k=1}^{N} \left(\frac{F(\boldsymbol{\eta}_k) - y_k}{\beta_k} \right)^2 + \delta \int_{\Omega} (\Delta_{\boldsymbol{\eta}}^* F(\boldsymbol{\eta}))^2 d\omega(\boldsymbol{\eta})$$
(73)

is minimized in $H^{(2)}(\Omega)$, where β_k are given positive weights and $\delta \geq 0$ an arbitrary parameter, which give a measure for the desired smoothness (for more details concerning smoothness see [3]).

Remark 2.3.

Choosing $\delta=0$ in the spherical spline approximation method leads to strict interpolation.

Theorem 2.6.

Let δ , β_1, \ldots, β_N be given positive constants and (η_k, y_k) , $1 \le k \le N$ be given data points. Then there exists a unique spline function $S \in \mathcal{S}(\eta_1, \ldots, \eta_N)$ such that the inequality

$$\sigma_{B,\delta}(S) < \sigma_{B,\delta}(F)$$
 (74)

is valid for all $F \in H^{(2)}(\Omega)$ with equality only if F = S. Further on, if S is given by Definition 2.7, then S is uniquely determined by the equation system

$$S(\boldsymbol{\eta}_k) + \delta \beta_k^2 a_k = y_k \qquad (k = 1, \dots, N). \tag{75}$$



	δ=0	δ=10-5	δ=10-4	δ=10⁻³	δ=10-2	δ=10 ⁻¹	δ=10⁰
condition for n=100	7,5262*10 ⁶	8,8420*10 ⁵	1,7697*10 ⁵	1,0267*10 ⁵	2,4963*10 ⁴	1,2302*10³	12,85
condition for n=1000	2,2019*10 ¹⁴	6,5501*10 ⁷	5,5149*10 ⁶	2,4274*10 ⁶	6,8239*10 ⁵	4,0629*10 ⁴	670,08
condition for n=6000	1,6900*10 ¹⁶	3,2347*10 ⁸	1,1966*10 ⁸	6,3276*10 ⁷	4,9563*10 ⁷	1,5428*10³	158,39
condition for n=12000	7,3958*10 ¹⁶	1,8897*10 ¹⁰	2,4297*10°	1,5511*10 ⁸	4,5924*10 ⁷	2,5740*10³	287,70

Figure 5. Condition of the linear equation system (76) for n randomly distributed data points on the sphere.

The proof of the last theorem can be found in either [4] or [6].

Remark 2.4.

Equation (75) can be rewritten in matrix formulation as

$$\begin{pmatrix} -\mathbf{G} + \delta \mathbf{B} & \mathbf{A}^{\mathsf{T}} \\ \mathbf{A} & 0 \end{pmatrix} \begin{pmatrix} a \\ c \end{pmatrix} = \begin{pmatrix} y \\ 0 \end{pmatrix}, \tag{76}$$

where \mathbf{G} , \mathbf{A} , a, c, y are defined as in the proof of Theorem 2.3 and

$$\mathbf{B} = \begin{pmatrix} \beta_1^2 & 0 \\ & \ddots & \\ 0 & & \beta_N^2 \end{pmatrix} . \tag{77}$$

It is obvious, that by adding the positive diagonal matrix $\bf B$ to $\bf G$, the condition of the linear equation system decreases dramatically even for small δ . An example for the condition of the linear equation system for randomly distributed data points on the sphere can be found in Figure 5.

3. Results

In this section, the spline approximation method introduced in the last section is applied to Radio Occultation data in order to produce illustrations demonstrating the vertical composition as well as the change in selected layers of the Earth's atmosphere over time. Further on, some pictures are produced in order to compare different years for a given season and layer among each other. The parameter used in the approximation is the temperature. Nevertheless, it should be observed, that any atmospheric parameter can be approximated by this method.

3.1. Zoom through the Atmosphere

In this part, illustrations were created, which show the temperature of the Earth's atmosphere, starting at $35 \, \text{km}$ height above mean sea level and zooming in to $7 \, \text{km}$ height above mean sea level in the time period June 2007 until August 2007, in order to show the vertical composition of the atmosphere. The time period is chosen in such a way, that the dataset is sufficiently large to smooth out short lived atmospheric states while maintaining the characteristics of the current season. The method used to calculate

the individual pictures is the smoothing spline approximation. The parameters have to be chosen in such a way, that they provide a balance between smoothing and representing the data exactly. Since all data points should be weighted equally, β_k was chosen to be equal to one for all k. Since the number of data points has a magnitude of circa $10^4,\,\delta=0.05$ seems a reasonable choice because it smooths the data sufficiently while still representing adequate detailed information. The pictures, which show the temperature of the Earth for selected altitudes in summer 2007, can be found in Figure 6.

Figure 7 shows that the temperature varies drastically. Starting at 35.0km altitude the temperature is located between $-59.5^{\circ}C$ and $-28.8^{\circ}C$ and drops until 21.2km altitude, while increasing the difference between the minimum ($-90.8^{\circ}\textit{C})$ and maximum value $(-42.9^{\circ}C)$ to $47.9^{\circ}C$. From 21.2km altitude to 16.2km, the minimum temperature starts to rise up to $-84.9^{\circ}C$, while the maximum temperature in those layers decreases further to $-44.0^{\circ}C$, which leads to a smaller difference of $-40.9^{\circ}C$ between minimum and maximum temperature. From there on up to 12.0km height, both, the minimum and maximum temperature increase again so that the temperature lies in the interval $[-76.8^{\circ}C, -42.9^{\circ}C]$ at 12.0km height. Since the minimum temperature increases faster as the maximum temperature, the difference between those temperatures decreases further to 33.9°C. In the final height interval between 12.0km and 7km altitude, the temperature increases further, but the difference between minimum $(-56.7^{\circ}C)$ and maximum value $(-12.7^{\circ}C)$ increases again to 44.0° C.

3.2. Approximation over Time

In this section, the dataset was interpolated over time in order to show the change of the temperature at $7 \, \mathrm{km}$ altitude over the seasons. Since the number of data points utilized in the approximation is significantly smaller than in the last section, the parameter δ can be chosen as $\delta=0.005$. This has the benefit that the produced graphical illustrations show more details as in the previous section. The same β_k are used as in the last section, $\beta_k=1$ for all k. All individual pictures consist of the data of seven consecutive days in order to provide a sufficient dense dataset and even out the influence from the day-night alteration. Figure 8 shows the plots of the temperature distribution at $7 \, \mathrm{km}$ altitude.

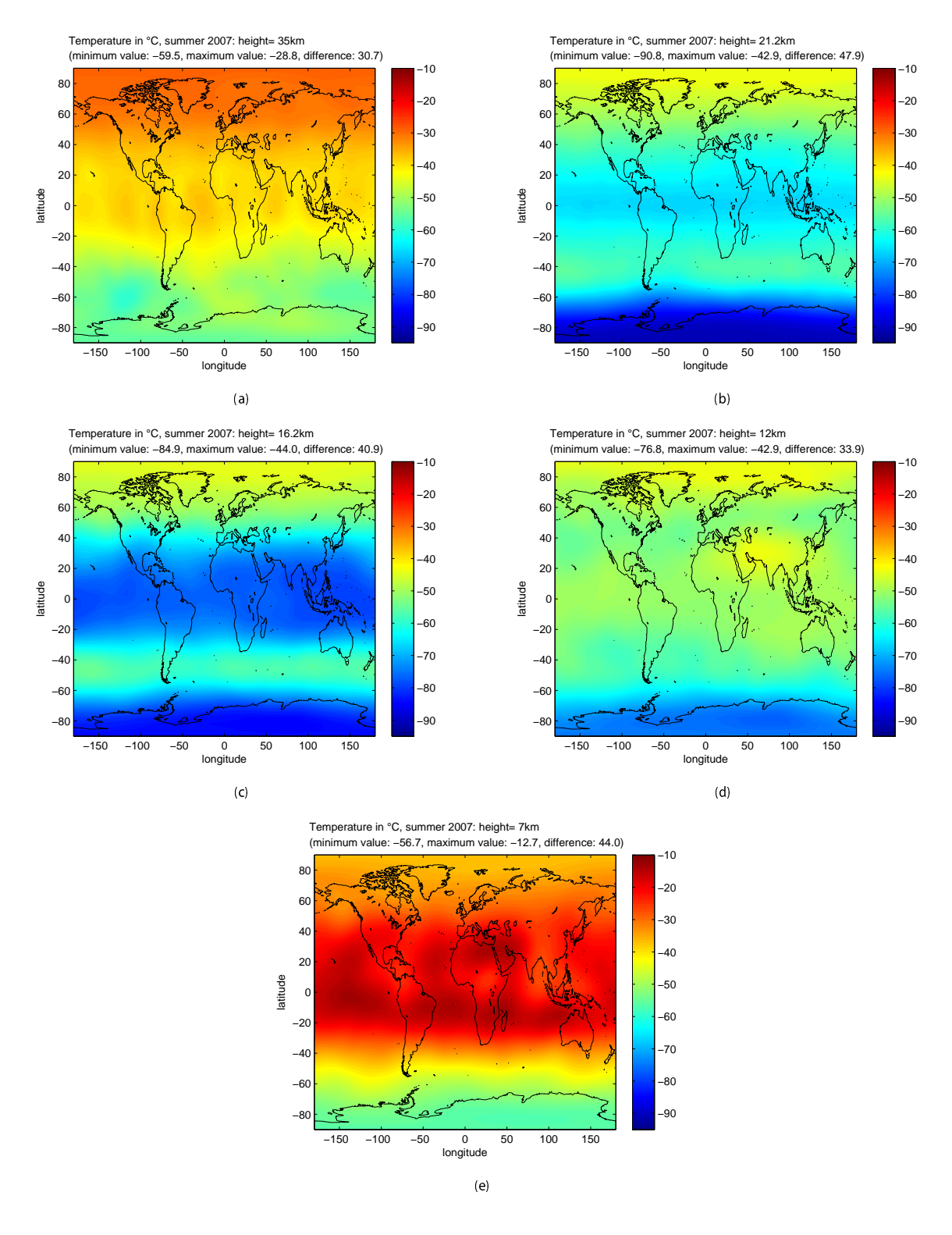


Figure 6. Temperature distribution in summer 2007 for selected heights.



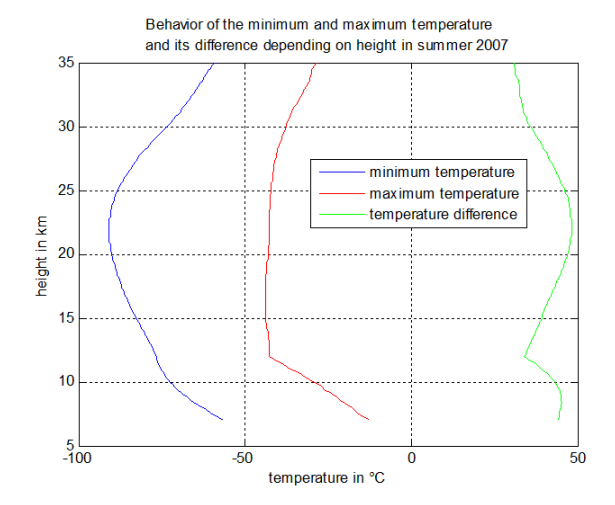


Figure 7. Behavior of the minimum and maximum values and its difference of the temperature in summer 2007.

3.3. Comparison of Different Years using Spherical Spline Approximation

The spherical spline approximation method is uniquely suited for the comparison of different years, since the comparison involves only the subtraction of the spline functions of the two different years. Hence, if the spline function is once computed for a given height, time period and year, it can be compared to any other year with the same time period and height. Figure 9 shows the temperature at 20km altitude in spring 2006 compared with the corresponding temperatures in spring in the years 2002 until 2008. The figure indicates, that, compared with the other years, the temperature above Greenland and North Canada in spring 2006 at 20km altitude was the lowest in the time period mentioned above, while the temperature at the south pole was the highest.

3.4. Computation of Atmospheric Profiles

By use of the spherical spline approximation method, we are able to compute atmospheric profiles for arbitrary locations on the Earth. In order to compute those profiles, the spherical spline function has to be computed for several layers of the Earth's atmosphere. The data at hand provides atmospheric profiles with measurements in 200m intervals. By computing the spherical spline function for each of those layers and evaluating this function at the desired position on the Earth, the atmospheric profile can be computed. Exemplary, a vertical temperature profile for Kaiserslautern, Germany was computed. The city is located at 49.424° N, 7.745° O. The nearest measurement is located at 50.514° N, 8.769° O, which corresponds to a distance of 141.23km to the desired location. For the calculation, all measurements in July 2007 were taken into account. The smoothing parameter δ was selected as 0.01. In order to weight the measurements close to the desired location,

the parameters β_k where selected as $2-\eta \cdot \eta_k$. The η_k indicate the positions of the measurements on the unit sphere, η the position of the desired location. The results of the computations can be seen in Figure 10.

4. Discussion

The results from the last section show, that the spherical spline approximation method is an adequate method for the approximation of the given Radio Occultation data. Further on, the numerical experiments showed, that the spherical spline method is numerically stable even for vast linear equation systems, which contributes further to the usefulness of the method. In addition, the parameters of the method provide a vast adaptivity for adjusting the method to a given approximation problem. It could be shown, that spherical splines are uniquely suited for approximating scattered data. However, as for any other method, the approximation can be improved by a larger dataset. The ideal dataset should consist of measurements, where all measurements taken within an hour would be evenly distributed over the whole sphere, which would require several measuring satellites.

Acknowledgement

Particular thanks goes to Dr. Jens Wickert from the GFZ (Geo-ForschungsZentrum) Potsdam, Germany for the provision of the vast amount of supplied Radio Occultation data, which was essential for this work. Dipl.-Math. C. Blick was financially supported by the "Board of Young Researchers" of the RP cluster of excellence " $(CM)^2$ " of the TU Kaiserslautern (Pl. W. Freeden).



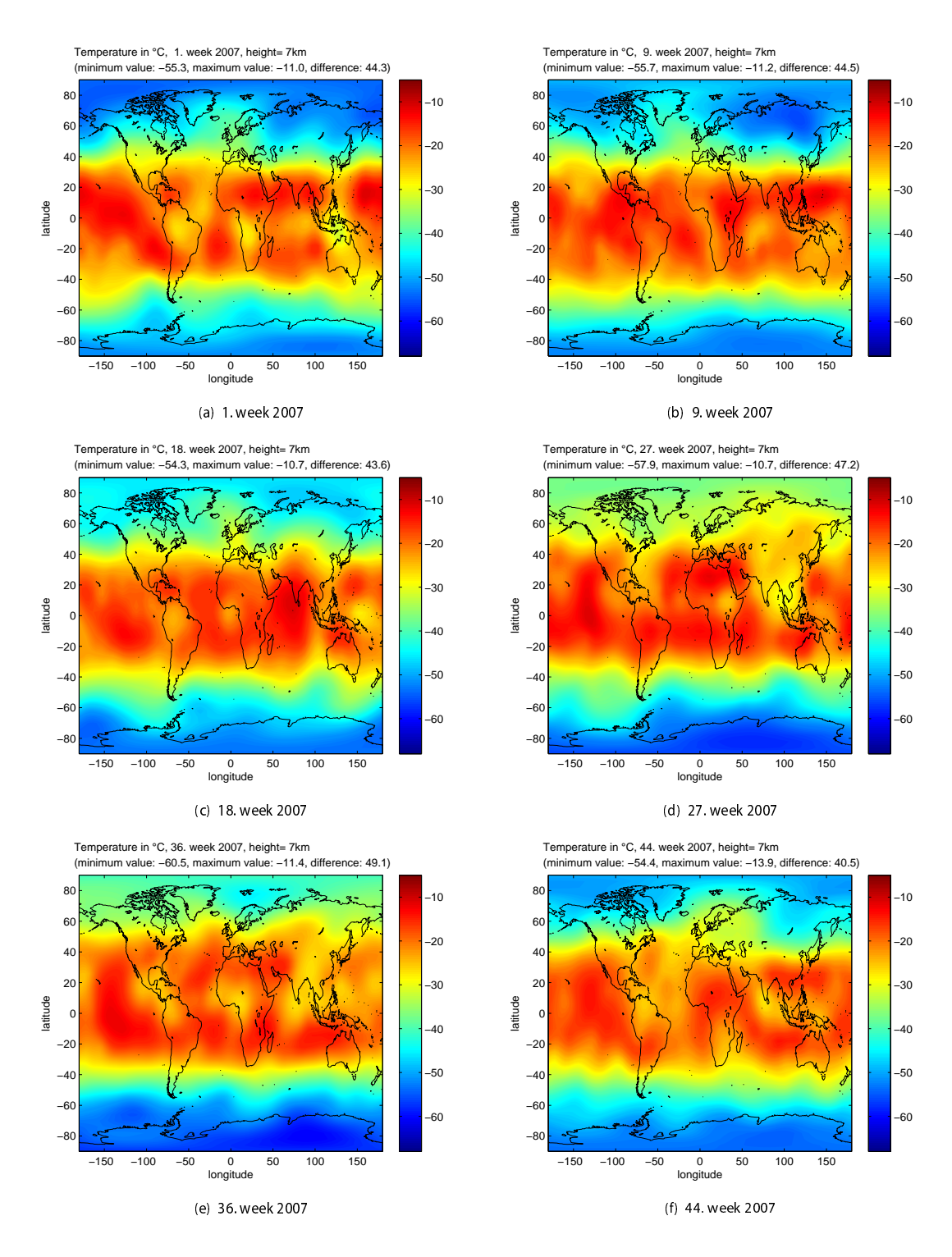


Figure 8. Temperature distribution at 7km altitude for selected times.



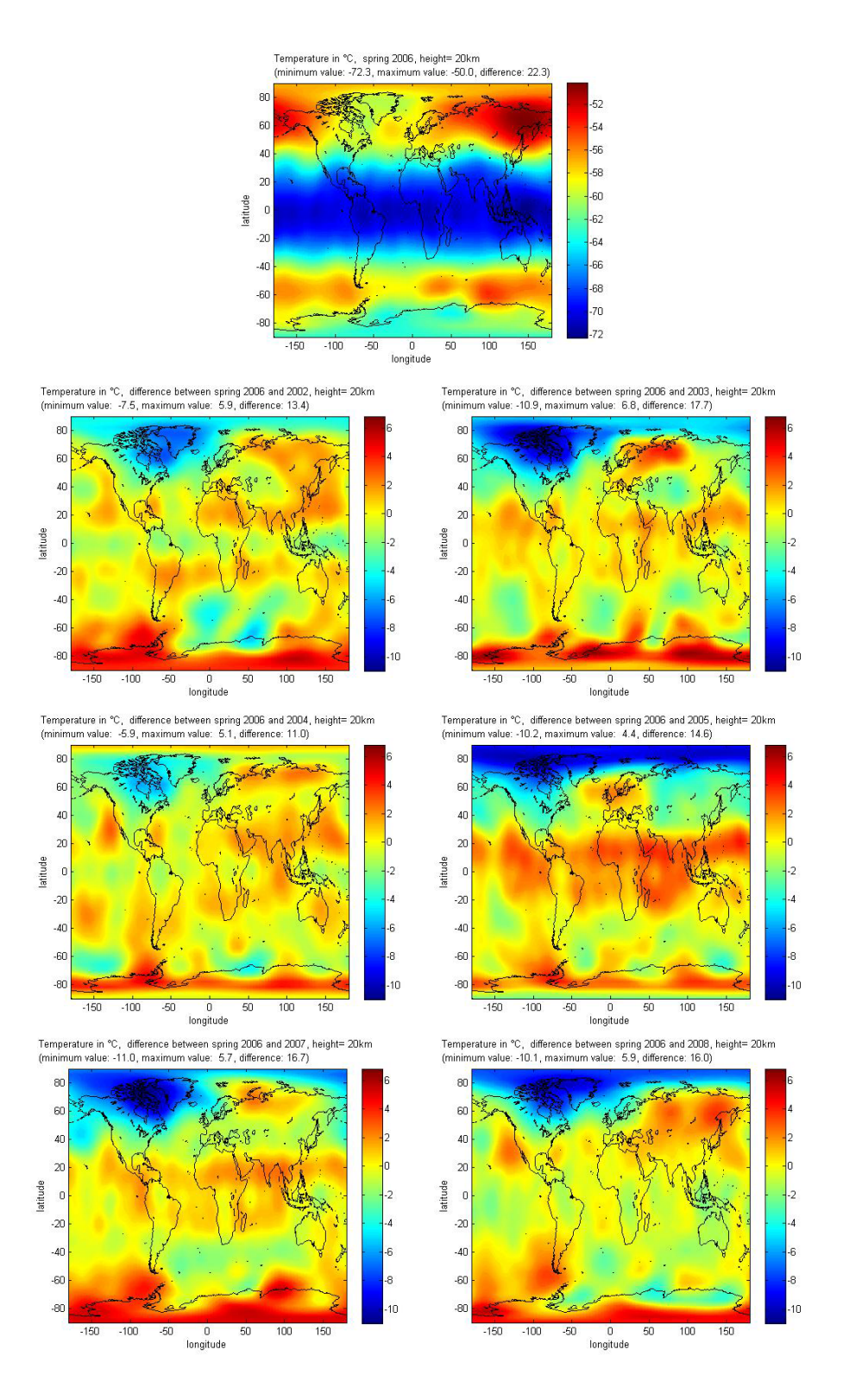


Figure 9. Temperature in spring 2006 (top) compared with the spring temperatures in 2002 to 2008 at 20km altitude.



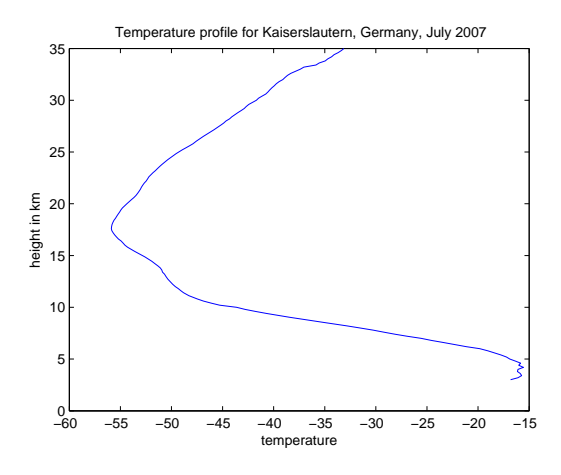


Figure 10. Temperature profile for Kaiserslautern, Germany in July 2007.

References

- [1] Anthes, R. A., Rocken, C., and Kuo, Y. H. (2000). Applications of COSMIC to Meteorology and Climate. Terr. Atmos. Oceanic Sci., 11:115--156.
- [2] Foelsche, U., Kirchengast, G., Steiner, A. K., Kornblueh, L., Manzini, E., and Bengtsson, L. (2008). An observing system simulation experiment for climate monitoring with GNSS radio occultation data: Setup and test bed study. Journal of Geophysical Research, 113.
- [3] Freeden, W. (1981a). On Approximation by Harmonic Splines.

 Manuscripta Geodaetica, 6:193--244.
- [4] Freeden, W. (1981b). On Spherical Spline Interpolation and Approximation. Math. Meth. in Appl. Sci., 3:551--575.
- [5] Freeden, W., Gervens, T., and Schreiner, M. (1998). Constructive Approximation on the Sphere with Application to Geomathematics. Clarendon Press.
- [6] Freeden, W. and Schreiner, M. (2009). Spherical Functions of Mathematical Geosciences - A Scalar, Vectorial and Tensorial Setup. Springer, 1st. edition.
- [7] Ge, S. (2006). GPS Radio Occultation and the Role of Atmospheric Pressure on Spaceborne Gravity Estimation over Antarctica. Report 479, The Ohio State University, Columbus, Ohio.
- [8] Gorbunov, M. E., Sokolovskiy, S. V., and Bengtsson, L. (1996).Space Refractive Tomography of the Atmosphere: Modeling

Journal of Geodetic Science

- of Direct and Inverse Problems. Report 210, Max Planck Institut of Meteorologie, Hamburg.
- [9] Gröbner, W. and Hofreiter, N. (1975). Integraltafel: Erster Teil, Unbestimmte Integrale. Springer, 5. edition.
- [10] Kursinski, E. R., Hajj, G. A., Schofield, J. T., Linfield, R. P., and Hardy, K. R. (1997). Observing Earth's atmosphere with radio occultation measurements using the Global Positioning System. Journal of Geophysical Research, 102:23,429--23,465.
- [11] Marquardt, C., Labitzke, K., Reigber, C., Schmidt, T., and Wickert, J. (2001). An Assessment of the Quality of GPS/MET Radio Limb Soundings during February 1997. Phys. Chem. Earth, 26(3):125--130.
- [12] Melbourne, W. G., Davis, E., Duncan, C., Hajj, G. A., Hardy, K., Kursinski, E., Meehan, T., and Young, L. (1994). The Application of Spaceborne GPS to Atmospheric Limb Sounding and Global Change Monitoring. Publication 94-18, Jet Propulsion Laboratory, Pasadena, California.
- [13] Reigber, C., Luehr, H., and Schwintzer, P. (2002). CHAMP Mission Status. Adv. Space Res, 30(2):129--134.
- [14] Schmidt, T., Wickert, J., Marquardt, C., Beyerle, G., Reigber, C., Galas, R., and König, R. (2004). GPS radio occultation with CHAMP: an innovative remote sensing method of the atmosphere. Advances in Space Research, 33:1036--1040.
- [15] Smith, E. K. and Weintraub, S. (1953). The Constants in the Equation of Atmospheric Refractive Index at Radio Frequencies. Proceedings of the IRE, 41:1035--1037.
- [16] Steiner, A. K., Kirchengast, G., Borsche, M., and Foelsche, U. (2007). A multi-year comparison of lower stratospheric temperatures from CHAMP radio occultation with MSU/AMSU records. Journal of Geophysical Research, 112.
- [17] Ware, R., Exner, M., Feng, D., M.Gobunov, Hardy, K., Herman, B., Y, K., Meehan, T., Melbourne, W., C.Rocken, Schreiner, W., Sokolovskiy, S., Soltheim, F., Zou, X., Anthes, R., Businger, S., and Trenberth, K. (1996). GPS Sounding of the Atmosphere for Low Earth Orbit: Preliminary Results. Bull. Amer. Meteor. Soc., 77:19-40.
- [18] Wickert, J. (2002). Das CHAMP-Radiookkultationsexperiment: Algorithmen, Prozessierungssystem und erste Ergebnisse. PhD thesis, Karl-Franzens-Universität zu Graz. Scientific Technical Report STR02/07.
- [19] Yunck, T. P., Liu, C.-H., and Ware, R. (2000). A history of GPS sounding. Terrestrial, Atmospheric and Oceanic Science, 11:1–20.